2020 IEEE International Conference on Power Electronics, Drives and Energy Systems (PEDES)

Gauss-Newton: A Prediction-Error-Gradient based Algorithm to Track PMSM Parameters Online

Aravinda Perera
Department of Electric Power Engineering
Norwegian University of Science and Technology
Trondheim, Norway
aravinda.perera@ntnu.no

Roy Nilsen
Department of Electric Power Engineering
Norwegian University of Science and Technology
Trondheim, Norway
roy.nilsen@ntnu.no

***Abstract*— Online adaptation of temperature-sensitive motor parameters is of significance for the electric drives in reliability-critical applications. Recursive prediction error method (RPEM) is widely used for this purpose. Gauss-Newton Algorithm (GNA), a prediction-error-gradients based algorithm, is adopted in this paper to find RPEM-gains for the parameter identification. This paper first investigates the simultaneous identifiability of permanent magnet flux linkage (Ψ_m), and stator resistance (R_s) of interior permanent magnet synchronous machine (IPMSM) using both nonlinear observability theorem and RPEM. Subsequently, GNA is analyzed for its tracking capability, speed of convergence, need of gain-scheduling and computational demand in comparison to stochastic gradient (SGA), another algorithm of the same class, using steady and dynamic state simulations.**

***Keywords*— Gain-matrix, Gain-scheduling, observability, parameter identification, PMSM, variable speed drives**

I. Introduction

At the wake of electrification in the safety-critical industries as such as seabed mineral mining, aerospace and offshore oil and gas, the dependability of the electrical systems becomes of major significance. PMSM equipped electric drives is a frontrunner in such applications due to its superior efficiency, power density, ease of cooling, design capability for fault-tolerance and good control dynamics in a wide torque-speed range [1] [2].

The accurate information of motor parameters is essential to ensure precise and adaptive control, condition monitoring, fault diagnosis and self-commissioning of high-performance variable speed drives. Moreover, the state-of-the-art industrial drives employ mechanical transducer-less control for reliability enhancement which demand accurate knowledge of electrical parameters of the machine in order to successfully estimate the rotor position. However, in practice, the exact physical parameters of the motor across its operating range are unavailable. Certain information can be obtained from the manufacturer which are often estimated with offline experiments in static operating conditions. Also, the electrical parameters of the motors can change due to either or a combination of the causes like operating point, ambience and faults of the drive. The effect of unaccounted parameter-variations can be sometimes fatal and often degrade the drive performance. Adding supplementary sensors in the PMSM for real time parameter acquisition is either not permitted or otherwise, requires cumbersome certification processes. Resorting only to sensors however can undermine the fail-safe nature of the drive.

Consequently, the estimation of IPMSM electric parameters, namely, Ψ_m, R_s , d- and q- axis inductances L_d and L_q, using offline and online methods has gained attention. Temperature and magnetic saturation are the main phenomena that affect parameter perturbations and Ψ_m and R_s are the main victims of them. On the other hand, not all electric parameters can be estimated simultaneously due to the rank-deficiency problem of IPMSM [3], [4] unless special efforts as in [5], [6], [7] are applied. Despite the importance of accurate knowledge of L_q and L_d, in practice, it is fair to estimate them offline because their potential impairment is caused by the stator current, a measured quantity, unlike the temperature-dependent parameters that can be varied due to unprecedented circumstances. Therefore, in this letter, online identification of Ψ_m, R_s is focused.

Prevalent online estimation methods are reviewed in [8], in which MRAS [9], [10], Kalman Filter (KF) [11] and recursive least square (RLS) [12], [5] -based methods appear to be the common approaches. Recursive prediction error method (RPEM), a generalized approach where RLS and KF based methods become its special cases [13], is adopted in the proposed method. Gauss-Newton algorithm is one applicable sub-algorithm inside RPEM for the identification of gain-matrix [13] which eventually determines the efficiency of parameter-tracking. Previously in [14], and [15], authors examined a similar sub-algorithm known as stochastic gradient (SGA) for the same cause in which it was evident that a zonal gain-scheduling scheme (ZGS) is indispensable in dealing with SGA to prevent undue adaptations because of the cross-coupling between Ψ_m and R_s. This paper investigates if GNA is intelligent enough to overcome the inherent parameter coupling such that the price of ZGS [16] can be circumvented. Furthermore, the speed of convergence and computational and programming complexity are evaluated of GNA in comparison to SGA with and without a ZGS.

II. Motor & Estimation Models

A. IPMSM Dynamic Model

The mathematical model of the electrical part of the machine is in the rotor co-ordinates, when given in the per-unit (pu) system:

$$\underline{u}_s^r = r_s \cdot \underline{i}_s^r + \frac{1}{\omega_n}\frac{d\underline{\psi}_s^r}{dt} + \mathbf{j}\cdot f_k \cdot \underline{\psi}_s^r, \quad \underline{\psi}_s^r = \mathbf{x}_s^r \cdot \underline{i}_s^r + \underline{\psi}_m^r$$
$$\underline{i}_s^r = [i_d \quad i_q]^T \quad \underline{\hat{\psi}}_m^r = [\hat{\psi}_m \quad 0]^T \quad \mathbf{x}_s^r = \begin{bmatrix} x_d & 0 \\ 0 & x_q \end{bmatrix} \quad \mathbf{j} = \begin{bmatrix} 0 & -1 \\ 1 & 0 \end{bmatrix} \tag{1}$$

Here, ω_n is the nominal rotational frequency. ϑ is the electrical angle of the mechanical position $p*\vartheta_{mech}$, where p is the number of pole pairs. Electrical speed is denoted by n. The superscript and subscript denote the reference frame and the location of the quantity (s-stator, r-rotor, m-magnet) respectively.

B. Parameter Identifiability

The weak, local observability theorem proposed for nonlinear dynamic systems in [17] is applied for observability

2020 IEEE International Conference on Power Electronics, Drives and Energy Systems (PEDES) | 978-1-7281-5672-9/20/$31.00 ©2020 IEEE | DOI: 10.1109/PEDES49360.2020.9379424

analysis of IPMSM in [4], where the authors establish a unified approach for position and speed observability. The theorem is extended in [7] to analyze the parameter-identifiability of IPMSM. In this section, it is adopted for the pu-model of IPMSM (1) in order to investigate simultaneous identifiability of ψ_m and r_s, the pu values of the respective quantities. Accordingly, a system's local and weak observability can be evaluated by using the rank of $\boldsymbol{O}$, the Jacobian (3) of the Lie derivative (2). For a nonlinear dynamic system of Lie derivative of the function h with respect to the vector field f is given by:

$$L_f h = (\nabla h) f = \frac{\partial h}{\partial x} f = \sum_{i=1}^{n} \frac{\partial h}{\partial x_i} f_i \qquad (2)$$

$$L_f^0 h = h \quad L_f^k h = L_f L_f^{k-1} h$$

Then $\boldsymbol{O}$, the Jacobian Matrix of the Lie derivatives become, where k is the order of the system:

$$\mathbf{O} = \frac{\partial}{\partial x}\left[L_f^0 h \quad L_f^1 h \quad \ldots \quad L_f^{k-1} h \right]^T \qquad (3)$$

If $\boldsymbol{O}$ has full rank as given in (4), it is guaranteed that the nonlinear system is weakly, locally observable [4], [17].

$$rank\{\mathbf{O}\} = k \qquad (4)$$

However, (4) is only a sufficient but not necessary condition, meaning, the IPMSM-states and parameters may be observable even if these conditions are not satisfied [4]. Often, $\boldsymbol{O}$ for electric drives is a complicated matrix in which the rank assessment is a tedious task, thus the general practice is to choose a regular submatrix of size k to check the above condition [3], [4].

As a first step, system model (1) can be extended to include ψ_m and r_s to make the system function, f as given in (5).

$$f_1 : \frac{di_d}{dt} = -\frac{r_s \cdot \omega_n}{x_d} \cdot i_d + n \cdot \frac{x_q \cdot \omega_n}{x_d} \cdot i_q + \frac{\omega_n}{x_d} \cdot u_d$$

$$f_2 : \frac{di_q}{dt} = -\frac{r_s \cdot \omega_n}{x_q} \cdot i_q - n \cdot \frac{x_d \cdot \omega_n}{x_q} \cdot i_d - n \cdot \frac{\psi_m \cdot \omega_n}{x_q} + \frac{\omega_n}{x_q} \cdot u_q \qquad (5)$$

$$f_3 : \frac{d\psi_m}{dt} \simeq 0,\ f_4 : \frac{dr_s}{dt} \simeq 0$$

Eq (5) assumes the variations of ψ_m and r_s are very slow compared to the current variations, which is a fair assumption, given the large thermal capacity. Also, ϑ, n, x_d, x_q are assumed known and the latter three quantities are assumed constant. Thus, the new state vector, $\underline{x}$ becomes:

$$\underline{x} = \left[i_d \quad i_q \quad \psi_m \quad r_s \right]^T \qquad (6)$$

The input and the output vectors $\underline{u}$ and $\underline{h}$ become:

$$\underline{u} = \left[u_d \quad u_q \right]^T \quad \underline{h} = \left[i_d \quad i_q \right]^T \qquad (7)$$

The system order, $k_{mot} = 4$, therefore, the order of $\boldsymbol{O}$ is 8x4 as given in (8). A submatrix, $\boldsymbol{O}_1$ is then chosen out of (8) as given in (10) which is solved for the respective elements where certain elements are presented in (9). Since the stator current is measured, we can ignore the first two columns, which correspond to i_d and i_q, for the sake of convenience [7], thus the submatrix that is relevant for the ψ_m and r_s identifiability becomes as in (11), and the required rank becomes 2, to ensure simultaneous identifiability of ψ_m and r_s. Close inspection of (11) tells that, for $\boldsymbol{O}_2$ to be full rank, which means to be able to identify both ψ_m and r_s-estimates simultaneously, the condition $n \neq 0$ and $i_d \neq 0$ must be fulfilled. At zero speed, only r_s-estimate can be identified, and this is guaranteed when $i_d \neq 0$. This implies that despite the average value of $i_d = 0$, with the help of persistent excitation to create the time derivate of $i_d \neq 0$, even at standstill, r_s can be estimated [7].

$$\mathbf{O} = \begin{bmatrix} \frac{\partial L_f^0 h_1}{\partial i_d} & \frac{\partial L_f^0 h_1}{\partial i_q} & \frac{\partial L_f^0 h_1}{\partial \psi_m} & \frac{\partial L_f^0 h_1}{\partial r_s} \\ \frac{\partial L_f^0 h_2}{\partial i_d} & \frac{\partial L_f^0 h_2}{\partial i_q} & \frac{\partial L_f^0 h_2}{\partial \psi_m} & \frac{\partial L_f^0 h_2}{\partial r_s} \\ \cdot & \cdot & \cdot & \cdot \\ \cdot & \cdot & \cdot & \cdot \\ \cdot & \cdot & \cdot & \cdot \\ \frac{\partial L_f^3 h_1}{\partial i_d} & \frac{\partial L_f^3 h_1}{\partial i_q} & \frac{\partial L_f^3 h_1}{\partial \psi_m} & \frac{\partial L_f^3 h_1}{\partial r_s} \\ \frac{\partial L_f^3 h_2}{\partial i_d} & \frac{\partial L_f^3 h_2}{\partial i_q} & \frac{\partial L_f^3 h_2}{\partial \psi_m} & \frac{\partial L_f^3 h_2}{\partial r_s} \end{bmatrix}_{8x4} \qquad (8)$$

$$\Omega_1 = 2\frac{r_s \cdot \omega_n}{x_d^2} \cdot i_d - n \cdot \frac{x_q \cdot \omega_n}{x_d^2} \cdot i_q - \frac{\omega_n}{x_d^2} \cdot u_d - n \cdot \frac{\omega_n}{x_d} \cdot i_q$$

$$\Omega_2 = 2\frac{r_s \cdot \omega_n}{x_q^2} \cdot i_q + n \cdot \frac{\omega_n}{x_q} \cdot i_d + n \cdot \frac{x_d \cdot \omega_n}{x_q^2} \cdot i_d - \frac{\omega_n}{x_q^2} \cdot u_q + n \cdot \frac{\omega_n}{x_q^2} \cdot \psi_m \qquad (9)$$

$$\mathbf{O}_1 = \begin{bmatrix} -\frac{r_s \cdot \omega_n}{x_d} & n \cdot \frac{x_q \cdot \omega_n}{x_d} & 0 & -\frac{\omega_n}{x_d} \cdot i_d \\ -n \cdot \frac{x_d \cdot \omega_n}{x_q} & -\frac{r_s \cdot \omega_n}{x_q} & -n \cdot \frac{\omega_n}{x_q} & -\frac{\omega_n}{x_q} \cdot i_q \\ \left(\frac{r_s^2}{x_d^2} - n^2 \right) \cdot \omega_n^2 & -\left(\frac{r_s \cdot x_q}{x_d^2} + \frac{r_s \cdot n}{x_d} \right) \cdot \omega_n^2 & -\frac{n^2 \cdot \omega_n^2}{x_d} & \Omega_1 \\ \left(\frac{r_s \cdot x_q}{x_q^2} + \frac{r_s \cdot n}{x_q} \right) \cdot \omega_n^2 & \left(\frac{r_s^2}{x_q^2} - n^2 \right) \cdot \omega_n^2 & \frac{r_s \cdot n \cdot \omega_n^2}{x_q^2} & \Omega_2 \end{bmatrix} \qquad (10)$$

$$\mathbf{O}_2 = \begin{bmatrix} -\frac{n^2 \cdot \omega_n^2}{x_d} & \Omega_1 \\ \frac{r_s \cdot n \cdot \omega_n^2}{x_q^2} & \Omega_2 \end{bmatrix} \qquad (11)$$

C. Online Parameter Estimation Model

The online parameter estimation (OPE) model proposed in [14], [15] is adopted in this letter which is presented in Fig. 1. The inherent sensitivities of this model to the model-parameter discrepancies will be profoundly utilized in the proposed parameter adaptation algorithm (PAA). The full-order model ($\mathcal{M}_{u\vartheta}$), is used with stator currents chosen as state variables (12). The rotor-oriented model is chosen for current prediction in the predictor.

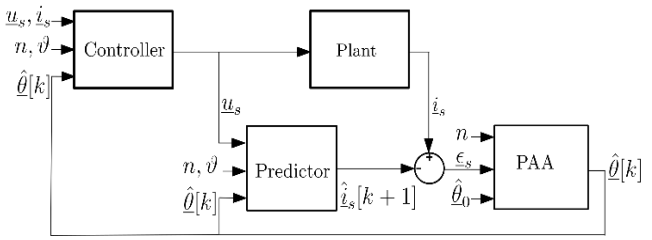

Fig. 1. Proposed online parameter estimation method block diagram

$$\underline{u}_s^r = \hat{r}_s \cdot \underline{\hat{i}}_s^r + \frac{\mathbf{x}_s^r}{\omega_n} \cdot \frac{d\underline{\hat{i}}_s^r}{dt} + \mathbf{j} \cdot n \cdot \hat{\mathbf{x}}_s^r \cdot \underline{\hat{i}}_s^r + \mathbf{j} \cdot n \cdot \underline{\hat{\psi}}_m^r \tag{12}$$

$$\hat{\underline{\theta}} = \begin{bmatrix} \hat{\psi}_m & \hat{r}_s \end{bmatrix}^T \quad \underline{i}_s^r = \mathbf{T}_{ss}^r(\vartheta) \cdot \underline{i}_s^s \qquad \underline{u}_s^r = \mathbf{T}_{ss}^r(\vartheta) \cdot \underline{u}_s^s$$

Here, from the estimated/model parameter matrix, $\hat{\underline{\theta}}$, $\hat{x}_d$, $\hat{x}_q$ are omitted to curtail the discussion only to scope of interest. As shown in (12), position and speed become inputs in the model, thus, they must be either measured or estimated. In this paper, a position sensor is assumed. In [16], this OPE is extended to position-sensorless control of IPMSM. $\mathscr{M}_{u\vartheta}$ is a second order system and the eigenvalues of this model are speed dependent. The system matrix **A** of the system can be expressed as:

$$\lambda \cdot I_2 - \mathbf{A} = \begin{bmatrix} \lambda + \frac{\omega_n \cdot \hat{r}_s}{\hat{x}_d} & -\frac{\omega_n \cdot n \cdot \hat{x}_q}{\hat{x}_d} \\ \frac{\omega_n \cdot n \cdot \hat{x}_d}{\hat{x}_q} & \lambda + \frac{\omega_n \cdot \hat{r}_s}{\hat{x}_q} \end{bmatrix} \quad T_d = \frac{x_d}{r_s \cdot \omega_n}, T_q = \frac{x_q}{r_s \cdot \omega_n} \tag{13}$$

The eigenvalues become:

$$\lambda_{1,2} = -\frac{1}{2} \cdot \left(\frac{1}{\hat{T}_d} + \frac{1}{\hat{T}_q} \right) \pm \sqrt{\left(\frac{1}{2} \cdot \left(\frac{1}{\hat{T}_d} + \frac{1}{\hat{T}_q} \right) \right)^2 - \left(\frac{1}{\hat{T}_d \cdot \hat{T}_q} + (\omega_n \cdot n)^2 \right)} \tag{14}$$

D. Decoupling Technique

Despite ψ_m and r_s are identifiable simultaneously under certain conditions, these parameters are inherently coupled, and their coupling is given by f_2 in (5). It also tells that the ψ_m and r_s can be decoupled by keeping either $n = 0$ or $i_q = 0$ which is not practical in most of the operating points of the drive. The effect of coupling is analyzed in [16] where it was found out that due to ψ_m-estimate errors ($\delta\psi_m$), r_s-estimate gets heavily penalized because $r_s << \psi_m$ in per-unit. Due to this large asymmetricity in magnitudes, the penalty on ψ_m-estimate due to r_s-estimate errors (δr_s) is not considerable unless n is very small. The proposed ZGS in [16] circumvents the coupling issue with respect to ψ_m, but not w.r.t r_s, thus if ψ_m is erroneous in the r_s-adaptation zone, r_s gets unfairly compensated.

III. Parameter Adaptation Algorithm

A. Recursive Prediction Error Method

RPEM, a numerical estimation approach, is adopted as the PAA in this scope to recursively track ψ_m and r_s. RPEM in discrete form based on the Forward Euler Method, becomes, where D_M is the defined parameter space:

$$\hat{\underline{\theta}}[k] = \left[\hat{\underline{\theta}}[k-1] + \mathbf{L}[k] \cdot \underline{\varepsilon}_s^r[k] \right]_{D_M} ; D_M = \begin{Bmatrix} \psi_{m,\min} \le \hat{\psi}_m \le \psi_{m,\max} \\ r_{s,\min} \le \hat{r}_s \le r_{s,\max} \end{Bmatrix} \tag{15}$$

$\boldsymbol{L}$[k], the gain-matrix and $\underline{\varepsilon}^r{}_s$ in steady state, in component form, ε_d, ε_q are given in (16) and (17) respectively.

$$\mathbf{L}[k] = \begin{bmatrix} L_{11}[k] & L_{12}[k] \\ L_{21}[k] & L_{22}[k] \end{bmatrix}, \quad \begin{matrix} L_{11}, L_{12} = \text{gains of } \hat{\psi}_m \\ L_{21}, L_{22} = \text{gains of } \hat{r}_s \end{matrix} \tag{16}$$

ε_d and ε_q in (17) indicate that, in combination to (15), irrespective of $\boldsymbol{L}$[k], when $n=0$, the ψ_m-estimate does not get updated although, r_s-estimate gets updated as long as $i_d \neq 0$ or $i_q \neq 0$. This inference not only corroborates the sufficient condition deduced from the identifiability analysis performed previously using the nonlinear observability theorem, but also discloses a necessary condition, that r_s can be estimated at $n=0$, if either or both i_d, $i_q \neq 0$, i.e. $i_s \neq 0$. In a different perspective, (17) also tells that the sensitivity of the $\underline{\varepsilon}^r{}_s$ to $\delta\psi_m$ also rises with rotor speed that results in accelerating the adaptation of ψ_m-estimate as per (15). And the adaptation speed of r_s-estimate is both n and i_s -dependent hinting its adaptation is adaptive according to the load of the drive.

$$\begin{aligned} \varepsilon_d &= -\frac{n^2 \cdot \hat{x}_q}{\hat{r}_s^2 + n^2 \cdot \hat{x}_q \cdot \hat{x}_d} \cdot \delta\psi_m \\ &\quad - \left[\frac{\hat{r}_s}{\hat{r}_s^2 + n^2 \cdot \hat{x}_q \cdot \hat{x}_d} \cdot i_d + \frac{n \cdot \hat{x}_q}{\hat{r}_s^2 + n^2 \cdot \hat{x}_q \cdot \hat{x}_d} \cdot i_q \right] \cdot \delta r \\ \varepsilon_q &= -\frac{n \cdot \hat{r}_s}{\hat{r}_s^2 + n^2 \cdot \hat{x}_q \cdot \hat{x}_d} \cdot \delta\psi_m \\ &\quad - \left[\frac{\hat{r}_s}{\hat{r}_s^2 + n^2 \cdot \hat{x}_q \cdot \hat{x}_d} \cdot i_q - \frac{n \cdot \hat{x}_d}{\hat{r}_s^2 + n^2 \cdot \hat{x}_q \cdot \hat{x}_d} \cdot i_d \right] \cdot \delta r \\ \delta\psi_m &= \psi_m - \hat{\psi}_m, \ \delta r_s = r_s - \hat{r} \end{aligned} \tag{17}$$

IV. Search-Direction Algorithm

A. Introduction and Common Terms

A search-direction algorithm is required to efficiently identify the gain-matrix $\boldsymbol{L}[k]$ for accurate identification of $\hat{\underline{\theta}}$ in D_M. Gauss-Newton Algorithm comes into play in this regard. The stochastic gradient (SGA), an algorithm of the same context investigated for parameter-adaptation in [15], is evaluated here in parallel to create a basis of comparison. Before doing so, the common terms appearing in the algorithms are introduced. First is the prediction-error gradient (PEG, $\boldsymbol{\Psi}^T$), which is the heart of the above search-algorithms as they show conspicuous sensitivity to the model-parameters. The d- and q- axes components of the steady state PEGs are in (18) and (19) for ψ_m and r_s respectively and their plots are found in Fig. 2 and Fig. 3. By inspecting the expressions for PEGs, it is clear that they are independent of $\delta\psi_m$, and δr_s, unlike $\underline{\varepsilon}^r{}_s$.

Evidently, ψ_m-PEGs are zero at standstill, and its d-axis counterpart reaches a constant value equivalent to $\sim 1/x_d$ beyond zero-speed and thus, offers useful information in ψ_m-adaptation [15]. The r_s-PEGs, on the other hand, have relatively very high values at standstill (provided that $i_s \neq 0$)

$$\begin{aligned} \Psi_{11} &: \frac{d\hat{i}_d}{d\hat{\psi}_m} = -\frac{n^2 \cdot \hat{x}_q}{\hat{r}_s^2 + n^2 \cdot \hat{x}_q \cdot \hat{x}_d} \\ \Psi_{12} &: \frac{d\hat{i}_q}{d\hat{\psi}_m} = -\frac{n \cdot \hat{r}_s}{\hat{r}_s^2 + n^2 \cdot \hat{x}_q \cdot \hat{x}_d} \end{aligned} \tag{18}$$

$$\begin{aligned} \frac{d\hat{i}_d}{d\hat{r}_s} &= -\frac{\hat{r}_s}{\hat{r}_s^2 + n^2 \cdot \hat{x}_q \cdot \hat{x}_d} \cdot i_d - \frac{n \cdot \hat{x}_q}{\hat{r}_s^2 + n^2 \cdot \hat{x}_q \cdot \hat{x}_d} \cdot i_q \\ \frac{d\hat{i}_q}{d\hat{r}_s} &= -\frac{\hat{r}_s}{\hat{r}_s^2 + n^2 \cdot \hat{x}_q \cdot \hat{x}_d} \cdot i_q + \frac{n \cdot \hat{x}_d}{\hat{r}_s^2 + n^2 \cdot \hat{x}_q \cdot \hat{x}_d} \cdot i_d \end{aligned} \tag{19}$$

$$\Psi_{21} : \frac{d\left(\frac{d\hat{i}_d}{d\hat{r}_s}\right)}{dt} = -\frac{1}{T_d} \cdot \frac{d\hat{i}_d}{d\hat{r}_s} + \frac{\omega_n \cdot n \cdot \hat{x}_q}{\hat{x}_d} \cdot \frac{d\hat{i}_q}{d\hat{r}_s} - \frac{\omega_n}{\hat{x}_d} \cdot i_d \tag{20}$$

$$\Psi_{22} : \frac{d\left(\frac{d\hat{i}_q}{d\hat{r}_s}\right)}{dt} = -\frac{1}{T_q} \cdot \frac{d\hat{i}_q}{d\hat{r}_s} - \frac{\omega_n \cdot n \cdot \hat{x}_d}{\hat{x}_q} \cdot \frac{d\hat{i}_d}{d\hat{r}_s} - \frac{\omega_n}{\hat{x}_q} \cdot i_q$$

978-1-7281-5672-9/20/$31.00 ©2020 IEEE

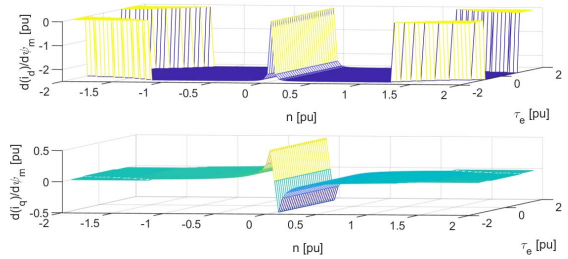

Fig. 2. Steady state d- and q- axis prediction-error gradients in the τ_e-n plane

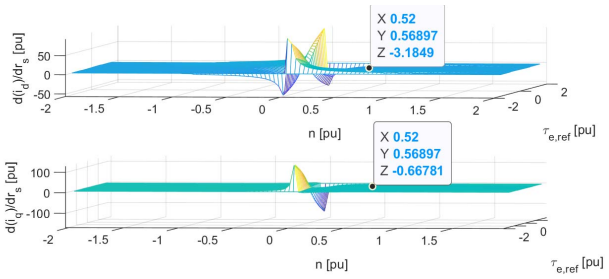

Fig. 3. Steady state d- and q- axis prediction-error gradients in the τ_e-n plane

and decay as rotor speed increases. It is also worth highlighting that, despite the rapid decay of r_s-PEGs when departing from zero-speed, their absolute values remain comparable with them in the ψ_m-PEGs implying the strong coupling between these parameters and the need for a decoupling mechanism for successful adaptation of r_s and ψ_m. In the computation of $\boldsymbol{L}[k]$ using GNA, the steady state solution of PEG for ψ_m-estimation (18) the and dynamic solution of PEG for r_s-estimation (20) are employed attributing to the same reasons discussed in [15] w.r.t SGA.

Hessian is another common quantity, which can take two forms, first the scalar form $r[k]$ in (21) formulated with the use of the traces of $\boldsymbol{\Psi}^T$ applied in SGA [15]. The matrix form of Hessian, $\boldsymbol{R}[k]$ (23) is applied in GNA, which makes one of the main differences between the algorithms. Furthermore, the Hessian can be either in filtered (or dynamic) form (23) or in unfiltered (or static) form as in (24). For the reasons discussed in [15], the filtered version is preferred for practical use whereas the unfiltered Hessian is used only for analysis.

B. Stochastic Gradient Algorithm

This algorithm is as follows, where scalar Hessian, $r[k]$ is employed:

$$\mathbf{L}[k]=\gamma[k]\cdot\frac{\boldsymbol{\Psi}[k]}{r[k]};\quad \gamma[k]=\gamma_0=\frac{T_{samp}}{T_0}$$

$$\boldsymbol{\Psi}^T=\left[\left(\frac{d\hat{i}_s^r\left[k,\hat{\psi}_m\right]}{d\hat{\psi}_m}\right)_{steady-state}\quad\left(\frac{d\hat{i}_s^r\left[k,\hat{r}_s\right]}{d\hat{r}_s}\right)_{dynamic-state}\right] \tag{21}$$

$$r[k]=r[k-1]+\gamma[k]\cdot\left\{tr\left[\boldsymbol{\Psi}[k]\cdot\boldsymbol{\Psi}^T[k]\right]-r[k-1]\right\}$$

$r[k]$ in steady state becomes:

$$r[k]=\left(\frac{d\hat{i}_d}{d\hat{\psi}_m}\right)^2+\left(\frac{d\hat{i}_q}{d\hat{\psi}_m}\right)^2+\left(\frac{d\hat{i}_d}{d\hat{r}_s}\right)^2+\left(\frac{d\hat{i}_q}{d\hat{r}_s}\right)^2 \tag{22}$$

C. Gauss-Newton Algorithm

The complete Gauss-Newton Algorithm is as follows:

$$\mathbf{L}=\gamma[k]\cdot\mathbf{R}[k]^{-1}\cdot\boldsymbol{\Psi}[k]\cdot\hat{\Lambda}^{-1}[k]$$
$$\mathbf{R}[k]=\mathbf{R}[k-1]+\gamma[k]\cdot\left\{\left[\boldsymbol{\Psi}[k]\cdot\hat{\Lambda}^{-1}[k]\cdot\boldsymbol{\Psi}^T[k]\right]-\mathbf{R}[k-1]\right\} \tag{23}$$

where the covariance matrix, Λ is taken as the identity matrix for simplicity in ensuing discussion. In steady state, $\boldsymbol{R}[k]$ becomes:

$$\mathbf{R}[k]=\boldsymbol{\Psi}[k]\cdot\boldsymbol{\Psi}^T[k] \tag{24}$$

The terms $\boldsymbol{\Psi}[k]$ and $\boldsymbol{R}[k]$ in steady state are as follows:

$$\boldsymbol{\Psi}[k]=\begin{bmatrix}\frac{d\hat{i}_d}{d\hat{\psi}_m}[k] & \frac{d\hat{i}_q}{d\hat{\psi}_m}[k]\\ \frac{d\hat{i}_d}{d\hat{r}_s}[k] & \frac{d\hat{i}_q}{d\hat{r}_s}[k]\end{bmatrix}=\begin{bmatrix}\Psi_{11} & \Psi_{12}\\ \Psi_{21} & \Psi_{22}\end{bmatrix} \tag{25}$$

$$\mathbf{R}[k]=\boldsymbol{\Psi}[k]\cdot\boldsymbol{\Psi}^T[k]$$
$$=\begin{bmatrix}\Psi_{11}^2+\Psi_{12}^2 & \Psi_{11}\cdot\Psi_{21}+\Psi_{12}\cdot\Psi_{22}\\ \Psi_{11}\cdot\Psi_{21}+\Psi_{12}\cdot\Psi_{22} & \Psi_{21}^2+\Psi_{22}^2\end{bmatrix}=\begin{bmatrix}R_{11} & R_{12}\\ R_{21} & R_{22}\end{bmatrix} \tag{26}$$

From inspection of (26), R_{22} is clearly the largest component until the mid-speeds, because it is the sum of squares of the largest PEGs (Ψ_{21}, Ψ_{22}) in the low-speed regions. Moreover, it is worth noting that, at standstill, R_{22} is the only nonzero term provided that $i_s \neq 0$.

Like KF-based approaches, GNA demands matrix computation including inversion. $\boldsymbol{R}^{-1}[k]$ in steady state becomes as follows:

$$\mathbf{R}^{-1}[k]=\frac{1}{|\mathbf{R}[k]|}\cdot\begin{bmatrix}R_{22} & -R_{12}\\ -R_{21} & R_{11}\end{bmatrix};\qquad R_{12}=R_{21} \tag{27}$$
$$|\mathbf{R}[k]|=\Psi_{11}^2\cdot\Psi_{22}^2+\Psi_{12}^2\cdot\Psi_{21}^2-2\cdot\Psi_{11}\cdot\Psi_{12}\cdot\Psi_{21}\cdot\Psi_{22}$$

Subsequently, the steady state $\boldsymbol{L}[k]$ is computed in which the elements are:

$$L_{11}=\frac{\gamma_0}{|\mathbf{R}[k]|}\cdot\left\{\Psi_{11}\cdot R_{22}-\Psi_{21}\cdot R_{12}\right\}$$
$$L_{12}=\frac{\gamma_0}{|\mathbf{R}[k]|}\cdot\left\{\Psi_{12}\cdot R_{22}-\Psi_{22}\cdot R_{12}\right\} \tag{28}$$
$$L_{21}=\frac{\gamma_0}{|\mathbf{R}[k]|}\cdot\left\{\Psi_{21}\cdot R_{11}-\Psi_{11}\cdot R_{12}\right\}$$
$$L_{22}=\frac{\gamma_0}{|\mathbf{R}[k]|}\cdot\left\{\Psi_{22}\cdot R_{11}-\Psi_{12}\cdot R_{12}\right\}$$

From inspection of (28), it can be expected that L_{11} and L_{12} will be the largest in the low-speed region owing to the large R_{22}. Thus, by nature of the GNA, the ψ_m-adaptation is expected to become rapider when the speed is low, in comparison to that in SGA. Yet, when the speed increases, due to the rapid decline of Ψ_{21}, and Ψ_{22}, the magnitude of R_{22} also declines, thus none of the gains in (28) will have an outstanding magnitude in the mid and high-speed regions. When standstill-behavior is concerned, all these elements in the $\boldsymbol{L}[k]$ become zero. This does not influence the ψ_m-adaptation as the $\underline{\varepsilon}^r_s$ anyway does not carry respective information. Contrastingly, $\underline{\varepsilon}^r_s$ does carry information about δr_s at zero speed (if $i_s \neq 0$) thus forcing L_{21} , and L_{22} to null at this point, prevents possible r_s-adaptation at standstill. This phenomenon indicates an inherent drawback in GNA that SGA does not display.

978-1-7281-5672-9/20/$31.00 ©2020 IEEE

D. Steady state analysis

To investigate the steady state behavior of key components of the formulae (21) and (28), a (-)10% steady state error (ε_d, ε_q when $\delta\psi_m$ = -10%) is analyzed in the torque-speed (τ_e-n) plane. ε_d, and ε_q are plotted in Fig. 4.

When $\boldsymbol{L}[k]$ computation is concerned, the magnitude of the respective denominators plays a role in the magnitude of the elements in $\boldsymbol{L}[k]$. In SGA, this is nothing but $r[k]$ (22) and the counterpart in GNA is the determinant of $\boldsymbol{R}[k]$, ($|\boldsymbol{R}[k]|$) (27). At zero-speed, $|\boldsymbol{R}[k]|$ becomes zero so are the elements of $\boldsymbol{R}[k]$ except R_{22}, thus the inverse yields zero-divided-by-zero scenarios in 3 of its elements. To tackle the challenge with non-existent inverse matrix due to these singularities at zero-speed, a mathematical method called Moore-Penrose pseudoinverse (MPP) is applied to find a pseudoinverse matrix which has most of the properties of $\boldsymbol{R}^{-1}[k]$ [18].

The two denominators, $r[k]$ and $|\boldsymbol{R}[k]|$ are plotted in the τ_e-n plane in the Fig. 5, that hold similar shapes except for the fact that $r[k]$ is several times larger up to ten times at most. The striking different between them is around the $n = 0$ axis, the former reaches its peak whereas the latter holds very low values (nearly zero) to create a cleavage between the peak wedges. At $n = 0$, $r[k] \neq 0$ and becomes the square of r_s-PEGs (see (22)) which are at their peaks as in Fig. 3. On the other hand, $|\boldsymbol{R}[k]|$ contains ψ_m-PEGs in its each term, which become zero at $n = 0$, thus, in theory, $|\boldsymbol{R}[k]|$ must be zero (but in practice, limited to very low values by MPP to avoid division by zero) at $n = 0$. In summary, $|\boldsymbol{R}[k]|$ offers higher boost in gain-computation at and around zero speed. Although, since GNA inherently prevents adaptation at zero-speed, the high boost offered by $|\boldsymbol{R}[k]|$ at standstill is futile.

In order to study the simultaneous adaptation mechanisms of SGA and GNA, the term $\boldsymbol{L}[k]\cdot\varepsilon_s$ in (15) that updates the old parameter value in the direction of adaptation, is useful. Let this term be known as the update-term, $q[k]$, which becomes for each parameter:

$$\begin{aligned} q_{\psi}[k] &= L_{11}[k]\cdot\varepsilon_d[k] + L_{12}[k]\cdot\varepsilon_q[k] \\ q_{r}[k] &= L_{21}[k]\cdot\varepsilon_d[k] + L_{22}[k]\cdot\varepsilon_q[k] \end{aligned} \tag{29}$$

For SGA, (29) becomes:

$$\begin{aligned} q_{1\psi}[k] &= \frac{\gamma_0}{r[k]}\left(\Psi_{11}[k]\cdot\varepsilon_d[k] + \Psi_{12}[k]\cdot\varepsilon_q[k]\right) \\ q_{1r}[k] &= \frac{\gamma_0}{r[k]}\left(\Psi_{21}[k]\cdot\varepsilon_d[k] + \Psi_{22}[k]\cdot\varepsilon_q[k]\right) \end{aligned} \tag{30}$$

For GNA, this becomes, where L-terms from (28):

$$\begin{aligned} q_{2\psi}[k] &= \left(L_{11}[k]\cdot\varepsilon_d[k] + L_{12}[k]\cdot\varepsilon_q[k]\right) \\ q_{2r}[k] &= \left(L_{21}[k]\cdot\varepsilon_d[k] + L_{22}[k]\cdot\varepsilon_q[k]\right) \end{aligned} \tag{31}$$

These terms are plotted for two cases; case-1: only ψ_m-error ($\delta\psi_m$=-10%), case-2: only r_s-error (δr_s=10%). Fig. 6 and Fig. 7 correspond to the case-1 with SGA and GNA respectively while, the Fig. 8 and Fig. 9 for the case-2, for SGA and GNA. In case-1, irrespective of the algorithm and τ_e, $q_\psi[k]$, $q_r[k]=0$ at zero-speed. Since $\underline{\varepsilon}^r{}_s = 0$ at this operating point, no adaptation is expected in either of the model parameters. When speed increases, $q_{1\psi}$, $q_{1r} \neq 0$ indicating an adaptation in

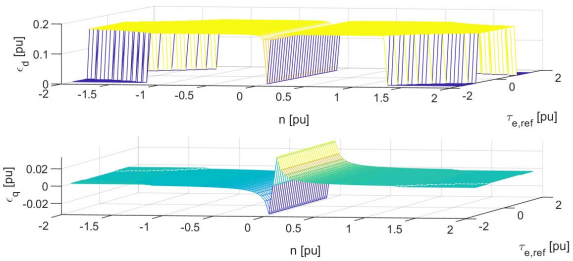

Fig. 4. Steady state d- and q- axis prediction-errors when $\delta\psi_m$ = -10% in the τ_e-n plane

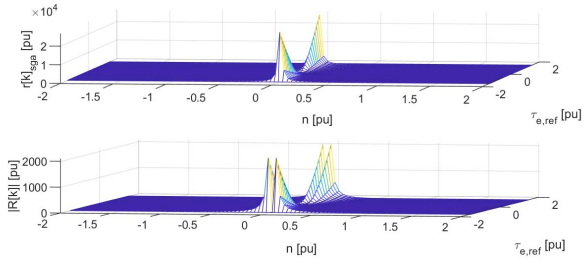

Fig. 5. Scalar Hessian, r[k] and the determinant of the matrix Hessian |R[k]|, both in steady state in τ_e-n plane

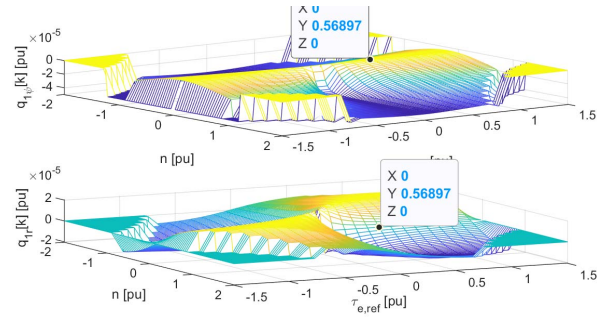

Fig. 6. The update-term in SGA when $\delta\psi_m$ = -10%, δr_s = 0, in τ_e-n plane

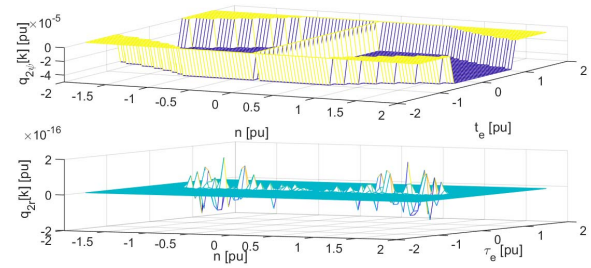

Fig. 7. The update-term in GNA when $\delta\psi_m$ = -10%, δr_s = 0, in τ_e-n plane

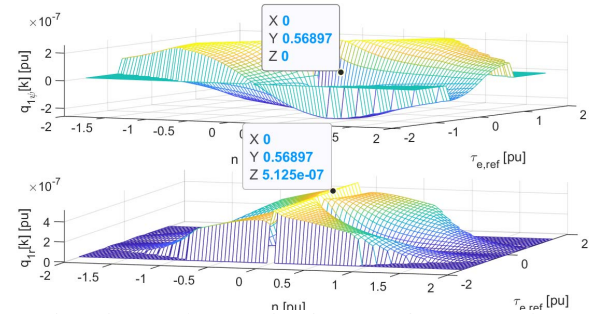

Fig. 8. The update term in SGA when δr_s = 10%, $\delta\psi_m$ = 0, τ_e-n plane

978-1-7281-5672-9/20/$31.00 ©2020 IEEE

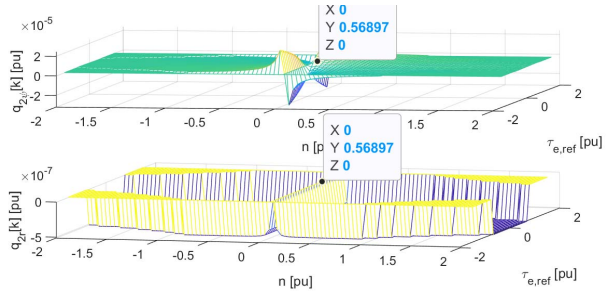

Fig. 9. The update term in GNA when $\delta r_s = 10\%$, $\delta\psi_m = 0$, τ_e-n plane

both parameters although the r_s-adaptation is undesirable. On the other hand, when GNA is concerned, $q_{2r}[k] \approx 0$ (in Fig. 7) to make the r_s-update minute in the presence of $\delta\psi_m$, which implies inherent decoupling, a favorable outcome. When case-2 is concerned, where only r_s-adaptation is expected, an inherent decoupling is evident neither in GNA nor SGA as in the respective figures. It is also interesting to notice, that at $n=0$, $q_{2r}[k] = 0$ but not $q_{1r}[k]$ to highlight the previously discussed drawback of GNA concerning non-adaptation at zero-speed.

V. Simulation Results & Discussion

A 3-phase IPMSM drive with a 2-level inverter and a constant load is simulated in MATLAB Simulink environment with Simscape toolbox. Asymmetrical modulation with 3rd harmonic injection is applied. The switching and the digital controller sampling frequencies are 3 kHz 6 kHz respectively. The dead-time effects in the inverter is compensated in the simulation. Maximum Torque Per Ampere (MTPA) -control strategy is used for the simulation with the aid of the 3rd order approximation for reference current calculations given in [14]. When the ZGS is applied, r_s-estimation occurs in the speed envelop -30 to 30 rpm whereas ψ_m-estimation from |300| to |3000| rpm.

TABLE I. Simulation Data

	Symbol	***Value***	***Unit***
Nominal voltage	U_N	690	V
Nominal current	I_N	478	A
Nominal frequency	f_N	50	Hz
Pole pairs	p	1	-
Rated torque	$\tau_{e,rated}$	1814.4	Nm
Nominal speed	N_{rated}	3000	rpm
Initial Motor parameter vector	$[\psi_m \; x_d \; x_q \; r_s]^T$	$[0.66\ 0.4\ 1\ 0.009]^T$	pu
Gain-sequence	γ_0	6.25e-4	pu

A. High Load-Torque Case

Both ψ_m and r_s of the motor vary twice during the time span at 1.2 s and 12.5 s as in Fig. 10. Assuming a temperature-increase, ψ_m-decrease and r_s-increase of 5% from the previous state is simulated. The load torque is kept at 0.8* $\tau_{e,rated}$ and the rotor speed varies as in the Fig. 11. Subplot-3 in Fig. 10 confirms the conclusion in [15], [16] that SGA without ZGS yields over-adaptation. However, the performance of GNA at the absence of scheduler is remarkable as in the subplot-1 of the same figure. The underlying phenomenon is explained shortly. The price of ZGS, however, is seen in the subplots-2 and 4, where parameters do not adapt until n enters the respective adaptation zones. This delay causes torque-error ($\delta\tau_e$) as seen in the subplots-2 and -3 in Fig. 11 that results in speed deviation. The rotor speed deviates to a level such that n reaches ψ_m-adaptation zone which initiates ψ_m-estimation that results in $\tau_{e,actual}$-correction. Note that the ZGS forces selected elements in the $\boldsymbol{L}[k]$ to zero thus for the understanding of natural dynamic behavior, subplots without the ZGS must be considered.

Update-terms in Fig. 12 tell that the $q_\psi[k]$ is about 100 times larger than $q_r[k]$. This difference is attributed to the disparity between $\delta\psi_m$, and δr_s in p.u. that is embedded in ε^r_s-term, despite the % change of parameters is the same. The $q[k]$-difference however does not cause over-adaptation in the r_s-estimate in GNA (subplot-1), unlike in SGA (subplot-3) even at the absence of the ZGS. This is because of the difference in $\boldsymbol{L}[k]$ computations in SGA and GNA discussed in the section IV and evident in the Fig. 13. At 1.2 s where the first parameter-change occurs, the tracking of GNA (without scheduler) is accurate because, at this point (mid-speed region), all four gain-elements have comparable sizes, unlike in SGA where $L_{21} + L_{22} > L_{12}$ that accelerates the r_s-adaptation to cause over-adaptation. At 12. 5 s (low-speed region), due to the R_{22}-effect, L_{11} and L_{12} are the largest in GNA (Fig. 13, subplot-1), therefore, even when both $\delta\psi_m$, $\delta r_s \neq 0$, ψ_m-adaptation occurs much rapidly than that for r_s. This is not valid in SGA, in which the magnitude of respective PEGs dictates the RPEM-gain of each parameter. In the low-speed region where Ψ_{21}, $\Psi_{22} > \Psi_{11}$, Ψ_{11} (see Fig. 14), r_s-estimate adapts before that of ψ_m in SGA, that causes over-adaptation due to the effect of $\delta\psi_m >> \delta r_s$.

As seen in the Fig. 15, in GNA, R_{22} is the largest and it remains nearly constant in the subplot-1 as the speed-region

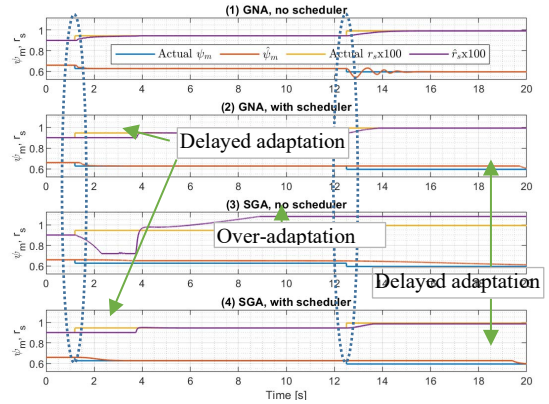

Fig. 10. Trajectories of estimated-ψ_m, r_s in the presence of varying motor parameters when applied (1), (2) GNA (3), (4) SGA

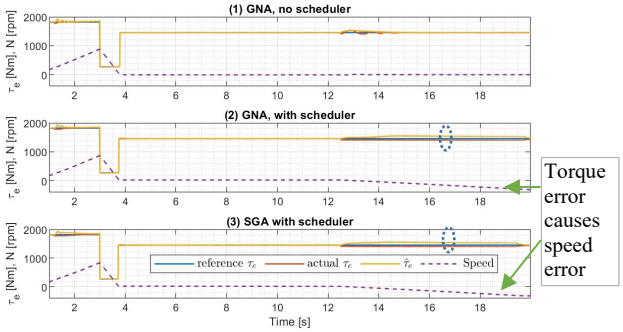

Fig. 11. The Reference, actual and estimated torques and speed in the drive

978-1-7281-5672-9/20/$31.00 ©2020 IEEE

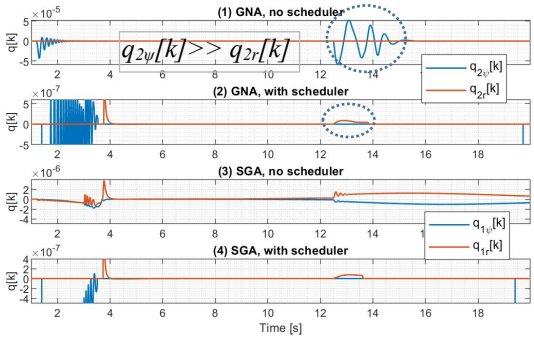

Fig. 12: Update terms' behavior in (1), (2) GNA (3), (4) SGA

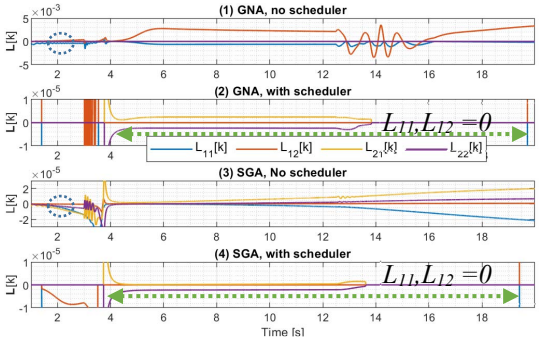

Fig. 13. **L**[k] behavior in (1), (2) GNA (3), (4) SGA

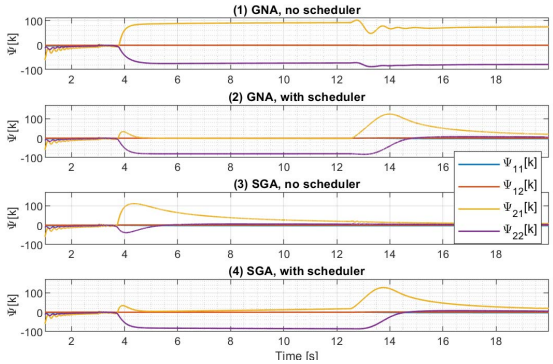

Fig. 14. PEGs' behavior in (1), (2) GNA (3), (4) SGA

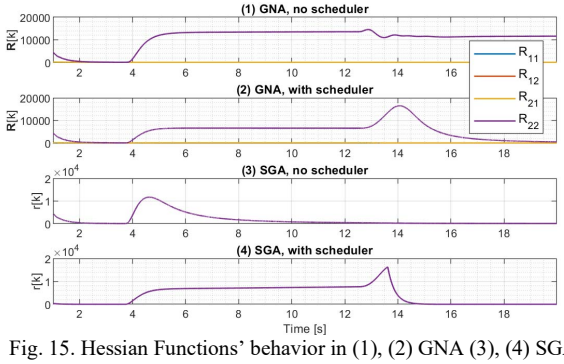

Fig. 15. Hessian Functions' behavior in (1), (2) GNA (3), (4) SGA

remain unchanged in the respective case, whereas, in subplot-2, due the consequential change of rotors-speed, the magnitudes of Ψ_{21}, Ψ_{22} diminish to decay the magnitude of R_{22}. Irrespective of the algorithm, Hessian is relatively very low in the mid to high-speed regions, due to the smaller PEG-values in these speed regions. To summarize, GNA in this simulation could perform simultaneous adaptation without the aid of the ZGS whereas SGA could not, thanks to the difference in the gain-computation in GNA. The tracking performance of the drive is indistinguishable between GNA and SGA when ZGS is applied.

B. *Low Load-Torque Case*

Here, r_s of the motor increases by 5% at 5 seconds and ψ_m decreases by 5% at 12.5 s. The load torque is kept at 0.1* $\tau_{e,rated}$ and the rotor speed varies across low to high speeds as in the Fig. 17. GNA without the scheduler shows undue adaptation of r_s-estimate at the presence of only $\delta\psi_m$ at 12.5 s in the subplot-1 in Fig. 16 whereas this undesired outcome is successfully prevented in the ZGS-applied cases. Moreover, such undue adaptation is not evident in the ψ_m-estimate at the presence of δr_s at 5 s.

In the no-ZGS cases in Fig. 18 (subplot-1,3) $q_\psi[k]$ has large values as expected after 12.5 s, but $q_r[k]$ also have rather small but considerable magnitudes undesirably, which are sufficient to make a conspicuous impact on the r_s-estimate due to its very small magnitude. Vice-versa coupling is seen at 5 s, in the presence of δr_s which anyway does not cause ψ_m to adapt unnecessarily, owing to its relatively large magnitudes in p.u. However, according to the steady state analysis in section IV-D such gains for r_s-adaptation is expected for SGA, but not for GNA. In looking at the gain-elements in Fig. 19, unlike the previous simulation case, here, all elements contain comparable magnitudes in the medium

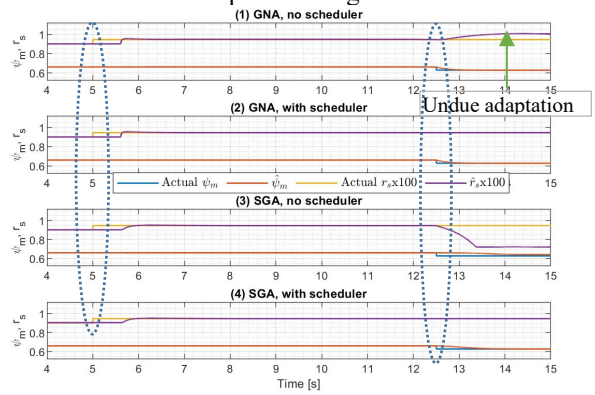

Fig. 16. Trajectories of estimated-ψ_m, r_s in the presence of varying motor parameters when applied (1), (2) GNA (3), (4) SGA

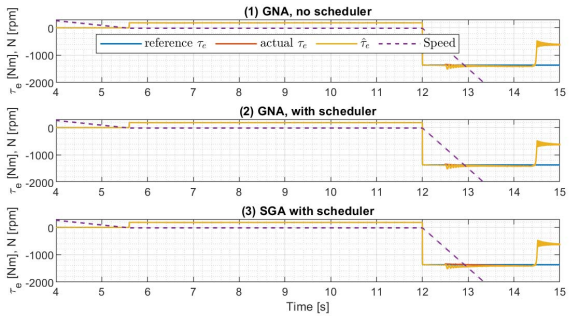

Fig. 17. The Reference, actual and estimated torques and speed in the drive

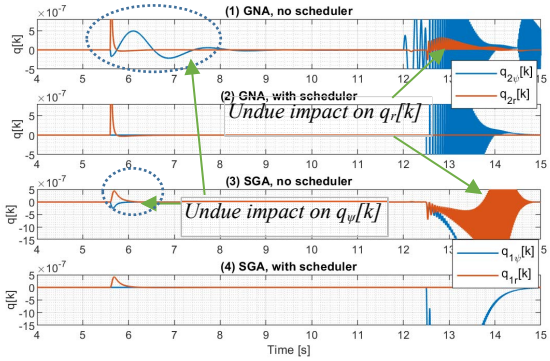

Fig. 18. Update-terms' behaviour in (1), (2) GNA (3), (4) SGA

978-1-7281-5672-9/20/$31.00 ©2020 IEEE

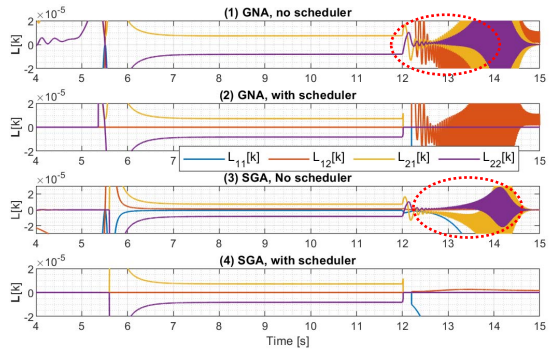

Fig. 19. **L**[k] behavior in (1), (2) GNA (3), (4) SGA

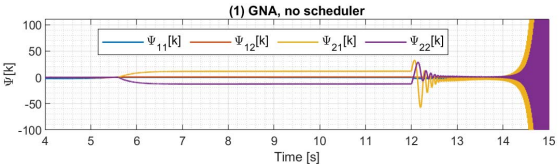

Fig. 20. PEGs' behavior in (1) GNA. SGA too yield a similar shape

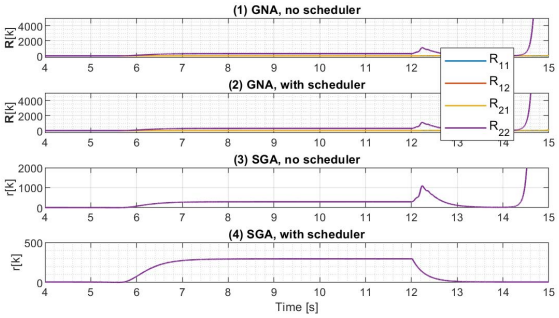

Fig. 21. Hessian Function behavior in (1), (2) GNA (3), (4) SGA

to high speeds because of the comparable magnitudes of PEGs in upper speeds shown in Fig. 20. A general remark: the high frequency oscillations seen beyond 12 s in the Fig. 18, 19 and 20 are attributing to the high rotor speeds that influence the speed-dependent eigenvalues in (14) which anyway do not interfere with the model parameter-adaptation trajectories as seen in the Fig. 16.

VI. CONCLUSION

This paper presents a recursive method for online adaptation of ψ_m and r_s of IPMSM using Gauss-Newton algorithm. Stochastic gradient algorithm is employed for the sake of comparing the figures of merit. GNA enables significantly rapider adaptation for ψ_m-estimate in the low-speed region in comparison to that of SGA. Thanks to this adaptation acceleration, when both parameters are erroneous, simultaneous adaptation is possible with GNA without the zonal gain-scheduling scheme. Although, when only ψ_m is erroneous, it was evident an undue adaptation-penalty on the r_s-estimate, due to the asymmetry of their per-unit magnitudes, which indicates that GNA needs to be accompanied by a zonal gain scheduler to ensure consistent tracking-performance across the operating region. It was also identified that GNA has inherent non-adaptation policy at standstill that prevents r_s-estimation possibly in a start-up estimation method which is possible with SGA. A numerical tolerance-assisted manipulation may help evade the non-adaptation at standstill, although its implementation in a digital controller could become a challenge. In general, the computational demand and complexity in implementation are substantial in GNA, with respect to SGA. On the other hand, GNA and SGA performances are indistinguishable when zonal gain-scheduler is applied. The use of time-dependent instead of static gain-sequence in order to augment GNA-performance can be an interesting further research work.

REFERENCES

[1] J. Holtz, "Acquisition of position error and magnet polarity for sensorless control of PM synchronous machines," *IEEE Trans. Ind. Appl.*, vol. 44, no. 4, pp. 1172–1180, 2008.

[2] A. G. Jack, B. C. Mecrow, and J. A. Haylock, "A Comparative Study of Permanent Magnet and Switched Reluctance Motors for," *IEEE Trans. Ind. Appl.*, vol. 32, no. 4, pp. 889–895, 1996.

[3] T. Boileau, N. Leboeuf, B. Nahid-Mobarakeh, and F. Meibody-Tabar, "Online identification of PMSM parameters: Parameter identifiability and estimator comparative study," *IEEE Trans. Ind. Appl.*, vol. 47, no. 4, pp. 1944–1957, 2011.

[4] P. Vaclavek, P. Blaha, and I. Herman, "AC drive observability analysis," *IEEE Trans. Ind. Electron.*, vol. 60, no. 8, pp. 3047–3059, 2013.

[5] S. J. Underwood and I. Husain, "Online parameter estimation and adaptive control of permanent-magnet synchronous machines," *IEEE Trans. Ind. Electron.*, vol. 57, no. 7, pp. 2435–2443, 2010.

[6] G. Feng, C. Lai, K. Mukherjee, and N. C. Kar, "Current Injection-Based Online Parameter and VSI Nonlinearity Estimation for PMSM Drives Using Current and Voltage DC Components," *IEEE Trans. Transp. Electrif.*, vol. 2, no. 2, pp. 119–128, 2016.

[7] S. Nalakath, M. Preindl, and A. Emadi, "Online multi-parameter estimation of interior permanent magnet motor drives with finite control set model predictive control," *IET Electr. Power Appl.*, vol. 11, no. 5, pp. 944–951, 2017.

[8] M. S. Rafaq and J. W. Jung, "A Comprehensive Review of State-of-the-Art Parameter Estimation Techniques for Permanent Magnet Synchronous Motors in Wide Speed Range," *IEEE Trans. Ind. Informatics*, vol. 16, no. 7, pp. 4747–4758, 2020.

[9] A. Piippo, M. Hinkkanen, and J. Luomi, "Adaptation of motor parameters in sensorless PMSM drives," *IEEE Trans. Ind. Appl.*, vol. 45, no. 1, pp. 203–212, 2009.

[10] A. Khlaief, M. Boussak, and A. Châari, "A MRAS-based stator resistance and speed estimation for sensorless vector controlled IPMSM drive," *Electric Power Systems Research*, vol. 108. pp. 1–15, 2014.

[11] R. Van Der Merwe and E. A. Wan, "The square-root unscented Kalman filter for state and parameter-estimation," *ICASSP, IEEE Int. Conf. Acoust. Speech Signal Process. - Proc.*, vol. 6, pp. 3461–3464, 2001.

[12] Y. Inoue, Y. Kawaguchi, S. Morimoto, and M. Sanada, "Performance improvement of sensorless IPMSM drives in a low-speed region using online parameter identification," *IEEE Trans. Ind. Appl.*, vol. 47, no. 2, pp. 798–804, 2011.

[13] L. Ljung and T. Soderstrom, *Theory and Practice of Recursive Identification*, 2nd Editio. Cambridge, Massachusetts: The MIT Press, 1985.

[14] A. Perera and R. Nilsen, "A Method Based on Prediction-Error-Gradients to Estimate PMSM Parameters Online," in *Conference Record - IAS Annual Meeting (IEEE Industry Applications Society)*, *In Press*, 2020, pp. 2–8.

[15] A. Perera and R. Nilsen, "A Framework and an Open-Loop Method to Identify PMSM Parameters Online," in *23rd International Conference on Electrical Machines and Systems, ICEMS, In Press*, 2020, p. 6.

[16] A. Perera and R. Nilsen, "A Sensorless Control Method for IPMSM with an Open-Loop Predictor for Online Parameter Identification," in *23rd International Conference on Electrical Machines and Systems, ICEMS, In Press*, 2020, p. 6.

[17] R. Hermann and A. J. Krener, "Nonlinear Controllability and Observability," *IEEE Trans. Automat. Contr.*, vol. 22, no. 5, p. 13, 1977.

[18] Mathworks, "Moore-Penrose pseudoinverse." [Online]. Available: https://www.mathworks.com/help/matlab/ref/pinv.html#mw_ffa95973-29a2-48a1-adb0-5a4214e0d9cf. [Accessed: 08-Oct-2020].

978-1-7281-5672-9/20/$31.00 ©2020 IEEE